International Journal of Solids and Structures 58 (2015) 257–269

Contents lists available at ScienceDirect

International Journal of Solids and Structures

journal homepage: www.elsevier.com/locate/ijsolstr

Modelling the mechanical aspects of the curing process of magneto-sensitive elastomeric materials

Mokarram Hossain [a], Prashant Saxena [a,b], Paul Steinmann [a,*]

[a] Chair of Applied Mechanics, University of Erlangen-Nuremberg, Egerlandstr. 5, 91058 Erlangen, Germany
[b] Center for Integrative Genomics, University of Lausanne, 1015 Lausanne, Switzerland

ARTICLE INFO

Article history:
Received 20 December 2013
Received in revised form 28 October 2014
Available online 17 January 2015

Keywords:
Magneto-sensitive polymers
Polymer curing
Finite strain
Magneto-mechanical coupled problem

ABSTRACT

In this paper, a phenomenologically motivated magneto-mechanically coupled finite strain elastic framework for simulating the curing process of polymers in the presence of a magnetic load is proposed. This approach is in line with previous works by Hossain and co-workers on finite strain curing modelling framework for the purely mechanical polymer curing (Hossain et al., 2009b). The proposed thermodynamically consistent approach is independent of any particular free energy function that may be used for the fully-cured magneto-sensitive polymer modelling, i.e. any phenomenological or micromechanical-inspired free energy can be inserted into the main modelling framework. For the fabrication of magneto-sensitive polymers, micron-size ferromagnetic particles are mixed with the liquid matrix material in the uncured stage. The particles align in a preferred direction with the application of a magnetic field during the curing process. The polymer curing process is a complex (visco) elastic process that transforms a fluid to a solid with time. Such transformation process is modelled by an appropriate constitutive relation which takes into account the temporal evolution of the material parameters appearing in a particular energy function. For demonstration in this work, a frequently used energy function is chosen, i.e. the classical Mooney–Rivlin free energy enhanced by coupling terms. Several representative numerical examples are demonstrated that prove the capability of our approach to correctly capture common features in polymers undergoing curing processes in the presence of a magneto-mechanical coupled load.

1. Introduction and outline

In recent years, the so-called magnetorheological elastomers (MREs) or magneto-active elastomers have obtained considerable attention as smart materials whose mechanical properties such as the shear modulus can be tuned by the application of an external magnetic induction. They consist of magnetically permeable particles embedded in a non-magnetic polymeric matrix. Mutual interactions between the particles and between the particles and the matrix are responsible for the macroscopic changes in the magnetomechanical properties of the elastomer. MREs are a relatively new group of smart materials. Due to their magnetically controllable stiffness and damping behaviour, they are attractive candidates for various technical applications. These applications range from automotive industry, e.g. suspension bushing, brakes, clutches, smart springs in dynamic vibration absorber to civil engineering devices such as building vibration isolators (Böse et al., 2012; Chen et al., 2007).

Magneto-sensitive polymers are prepared by dispersing micro-sized magnetically permeable particles in a non-magnetic matrix during the curing process. The most common ferromagnetic particle used is carbonyl iron (Böse et al., 2012; Boczkowska and Awietjan, 2009; Böse and Röder, 2009). Pure iron particle has the highest saturation magnetization of the known elements along with a high permeability and a low remnant magnetization, which provides high, short-term interparticle attraction (Boczkowska and Awietjan, 2009). The particle concentration varies between 0–30 percent, mainly expressed in terms of % by volume (Jolly et al., 1996). A high iron concentration may influence the long-term stability of the MRE materials. There are many materials that might be used as the matrix material of an MR composite. Most commonly used matrix elastomers are silicones or natural rubbers (Ginder et al., 2002; Lokander, 2004; Zhou, 2003). The shape and the size of the magnetically active filler particles have a major influence on the properties of an overall MR composite. Most often, spherical carbonyl iron particles with a diameter of several micrometres are used (Kaleta et al., 2011). As a result, the mechanical

* Corresponding author. Tel.: +49 09131 8528501; fax: +49 09131 8528503.
E-mail addresses: mokarram.hossain@ltm.uni-erlangen.de (M. Hossain), prashant.saxena@unil.ch (P. Saxena), paul.steinmann@ltm.uni-erlangen.de (P. Steinmann).

http://dx.doi.org/10.1016/j.ijsolstr.2015.01.010
0020-7683/

properties of these materials can be varied by the application of a magnetic field.

According to the way in which the magnetic particles are dispersed in the matrix as well as the magnetic induction is applied during the curing process, two kinds of MREs can be manufactured (Kaleta et al., 2011). Firstly, if the magnetic field is applied during the curing process anisotropic elastomers are produced where the magnetic particles are aligned strictly in a particular orientation, cf. Fig. (1, right). Polarized magnetorheological elastomers tend to show anisotropy in mechanical, magnetic and thermal properties (Jolly et al., 1996). Secondly, an isotropic elastomer composite will be formed when there will be no presence of the magnetic induction during the entire curing process, especially at the initial stage of the curing process, cf. Fig. (1, left). Such process of composite material formation will be characterized by a uniform particle distribution (Kaleta et al., 2011). It can be assumed that in the case of the isotropic magnetorheological composites, the magnetically active particles are dispersed homogeneously within the matrix. When a magnetic induction is applied after the fully-cured phase, the filler particles are not able to move freely due to the resistance offered by the cross-linked polymer structure. In such a situation, these particles tend to arrange themselves along the field vector direction. As result, a deformation of the matrix is observed, which can be interpreted as the magnetostriction. Scanning electron microscopy (SEM) can be used to observe MRE microstructure after the curing process. Here, we present both isotropic and transversally isotropic MREs that are produced using our laboratory facilities, cf. Fig. (1).

The deformations of elastomers are typically quite large. Hence the development of the constitutive model of such materials should be in a finite strain framework. The constitutive modelling of pure elastomers as well as magneto-sensitive polymers has a large amount of literature, see Boyce and Arruda (2000), Steinmann et al. (2012) and Hossain and Steinmann (2013) for reviews on the purely polymeric material modelling. The coupling between magnetism and nonlinear elasticity has generated much interest over last several decades which is reflected by variety of research publications in this area. The research of Eringen and Maugin (1990), Jackson (1975) and Pao (1978) are few important earliest works in this field. The works of Dorfmann and Ogden (2003, 2004), Brigadnov and Dorfmann (2003), Bustamante et al. (2007), Bustamante (2009, 2010), Saxena et al. (2013, 2014) and Kankanala and Triantafyllidis (2004) discussed mainly the constitutive relation of the nonlinear magneto-mechanical coupled problem while Vogel et al. (2013, 2012) and Miehe et al. (2011,) present the numerical implementation of coupled boundary value problems in the context of the finite element analysis. Several experimental results on magneto-mechanical coupled loadings are presented by Jolly et al. (1996), Kaleta et al. (2011) and Varga et al. (2006). Very recently, Danas et al. (2012) presented several experimental results and proposed a transversely isotropic energy density function that is able to reproduce the experimentally measured magnetization, magnetostriction and simple shear curves under different prestresses, initial particle chain orientations and magnetic fields.

In the curing process of polymers, a viscoelastic fluid transforms into a viscoelastic solid due to a series of chemical reactions. Such reactions result in polymer chains cross-linking to each other resulting in the formation of chemical bonds that allow the chains to come closer. Packing of chains due to cross-linking will yield a decrease in specific volume which is noted as the volume or curing shrinkage. During curing reactions with time, the viscosity and the stiffness of the liquid resin increase. The chemical reaction of the cross-linking polymers can be an exothermal reaction especially in the case of thermoset curing process, i.e. the formation of the polymer network is accompanied by a heat generation which is added to the external source of heating applied for the curing.

For an illustrative review on the constitutive modelling of the curing process of polymers, our previous works, cf. Hossain et al. (2009a, 2011, 2010) can be consulted. Only limited references for models for the evolution of viscoelastic properties during curing are available in the literature (Ruiz and Trochu, 2005; Suzuki and Miyano, 1977). In developing a cure-dependent small strain constitutive model for a thermosetting polymer, Kiasat (2000) assumed that the formation of new cross-links during curing does not affect the current stress state caused by previously applied strains, i.e. new cross-links form unstrained and stress-free. Several researches do agree with this assumption (Hojjati et al., 2004; Gillen, 1988). Lion and co-workers (Liebl et al., 2012a,b; Lion and Höfer, 2007; Lion and Johlitz, 2012; Lion et al., 2008; Lion and Yagimli, 2008) proposed a phenomenologically-inspired thermo-viscoelastic curing model for finite strains. This modular constitutive model includes thermally and chemically induced volume changes via a ternary multiplicative decomposition of the deformation gradient into mechanical, thermal and chemical parts. In order to realize the evolution of material parameters during curing, the so-called intrinsic time concept is introduced which is then related to the degree of cure. Yagimli and Lion (2011) reformulated their large strain model into a small strain version and validated it with sufficient experimental results.

Mergheim et al. (2012) developed a constitutive model to simulate the curing process-induced damage which evolves during the volume-shrinkage of curing in the case of a thermosetting material. They incorporated an isotropic gradient-enhanced damage model in small strain to describe the damage evolution. Very recently, Klinge et al. (2012a,b) proposed a multi-scale framework for the curing process modelling which deals with the viscoelastic curing together with the volume shrinkage. It is interesting to mention here that the works of Mergheim et al. (2012) and Klinge et al. (2012a,b) are mainly based on the hypoelastic framework for the curing modelling proposed by Hossain et al. (2009a,b, 2010), Hossain (2010) and Hossain and Steinmann (2011). Recently,

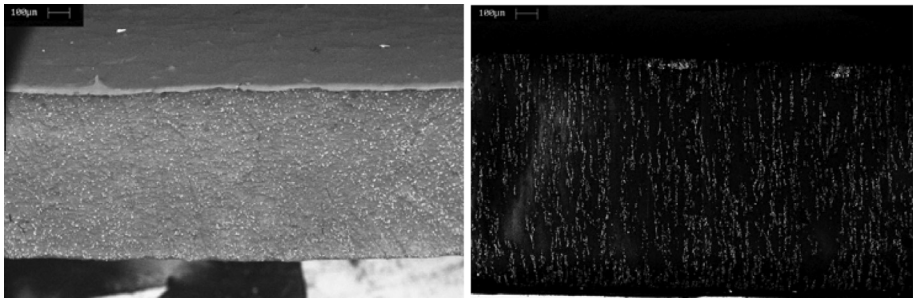

Fig. 1. SEM images (Courtesy of Bastian Walter) for 10% (by volume) iron-particle filled silicone elastomers; (Left) Isotropic MRE due to the absence of a magnetic induction during the curing process. (Right) transversally isotropic MRE produced under a magnetic induction applied in the vertical direction during the curing process.

Heinrich et al. (2013) proposed a thermo-chemo-mechanical coupled polymer curing model. They basically develop the model for the simulation of polymer curing processes during manufacturing of textile composites. The main assumption of their model is based on the notion of polymer networks that are continuously formed in a body of changing shape due to changes in temperature, chemistry and external loads. Moreover, a nonlinear damage model is also included to the main framework of the model.

Very recently, Mahnken (2013) proposed a macroscopic constitutive model for temperature-dependent visco-elastic effects in the case of curing. This thermodynamically consistent framework relies on an additive ternary decomposition of the logarithmic Hencky strain tensor into mechanical, thermal and chemical parts which is in contrast to the model of Lion and Höfer (2007) where the latter used a multiplicative decomposition of the deformation gradient into mechanical, thermal and chemical shrinkage parts. In this model, the concept of stoichiometric mass fractions for resin, curing agent and solidified material is used to derive the relations for the bulk compression modulus and the bulk heat- and shrinking dilatation coefficients.

Several experimental works demonstrate the formation of isotropic and anisotropic magneto-sensitive polymeric composites during curing process with or without the application of a magnetic induction. However, there is a lack of constitutive modelling, to the best of the authors' knowledge that can capture the curing process in the presence of a magnetic induction. Therefore, a finite strain framework is essential to predict the curing process with a magnetic field. The main framework of the proposed model is within the hypoelastic concept (rate-form) of our previously published purely mechanical curing model (Hossain et al., 2009a; Hossain and Steinmann, 2011; Hossain, 2010). A phenomenologically motivated convolution type potential function proposed here consists of three parts. i.e. a pure mechanical part, a pure magnetic part and a magneto-mechanical coupled part. The assumption introduced takes the fact into account that during the curing process all relevant material parameters are simultaneously experiencing a temporal evolution. In particular, this ansatz is not restricted to elasticity but can also be used for viscoelastic material models which will be discussed in a forthcoming contribution.

Section 2 discusses the main mathematical foundation that leads to a constitutive relation for the polymer curing process in the presence of mechanical and magnetic loadings. To apply the framework developed in Section 2, a free energy function that is frequently used for a fully-cured coupled magneto-elastic constitutive modelling is chosen and necessary derivations are given in Section 3. Evolutions of the various time-dependent material parameters appearing in the free energy function are discussed in Section 4. The final Section 5 presents some numerical examples demonstrating that the model proposed herein is well suited to reproduce relevant phenomena in the polymer curing in the presence of a magneto-mechanical coupled load.

2. Curing in magneto-elasticity

Elastic materials can be modelled using networks of springs each having a certain stiffness. Using a similar analogy, the continuous chain cross-linking within a curing polymer can be conceptualised as the addition of more and more springs to the network with time. Addition of more springs will increase the material stiffness and the stress development will also increase if there is an increment of loading continuously. A physical observation which has been reported in the literature is that a curing material, sustaining no current change of deformation, does not change its state of stress as resulted from previous deformations – even though its material properties continue to evolve. By the time the deformation state is changed again, the material properties that have evolved meanwhile define the new stress state, cf. (Kiasat, 2000; Gillen, 1988). Due to lack of experimental data, we take a similar assumption for the magnetic and coupled loadings. Such observation has to be taken into account in the development of the constitutive modelling of the curing process. Keeping the above mentioned physical fact in mind, a magneto-elastic coupled energy potential is proposed in the form of a convolution integral for the curing process in the presence of a magneto-mechanical coupled load as

$$\begin{aligned}\Phi(t) = &\frac{1}{2}\int_0^t \left[\boldsymbol{\mathcal{A}}'(s) : [\boldsymbol{F}(t) - \boldsymbol{F}(s)]\right] : [\boldsymbol{F}(t) - \boldsymbol{F}(s)]ds \\ &+ \frac{1}{2}\int_0^t [\boldsymbol{\mathcal{K}}'(s) \cdot [\mathbb{B}(t) - \mathbb{B}(s)]] \cdot [\mathbb{B}(t) - \mathbb{B}(s)]ds \\ &+ \int_0^t [\boldsymbol{\mathcal{C}}'(s) \cdot [\mathbb{B}(t) - \mathbb{B}(s)]] : [\boldsymbol{F}(t) - \boldsymbol{F}(s)]ds \end{aligned} \tag{1}$$

where $\boldsymbol{\mathcal{A}}'(s) = d\boldsymbol{\mathcal{A}}(s)/ds, \boldsymbol{\mathcal{K}}'(s) = d\boldsymbol{\mathcal{K}}(s)/ds$ and $\boldsymbol{\mathcal{C}}'(s) = d\boldsymbol{\mathcal{C}}(s)/ds$. In Eq. (1) $\boldsymbol{F}$ is the deformation gradient, $\mathbb{B}$ is the magnetic induction vector and t is the curing time. Note that $\boldsymbol{\mathcal{A}}, \boldsymbol{\mathcal{C}}, \boldsymbol{\mathcal{K}}$ are time-dependent fourth order, third order and second order magnetoelastic moduli tensors, respectively. Let $\mathcal{V}$ be a three dimensional Euclidian vector space and $\mathcal{T} = \mathrm{Lin}(\mathcal{V}, \mathcal{V})$ is a set of all linear transformations from $\mathcal{V}$ to $\mathcal{V}$. The energy function proposed in the Eq. (1) is reasonable if and only if the following conditions are satisfied

$$\left[\boldsymbol{\mathcal{A}}' : \boldsymbol{F}\right] : \boldsymbol{F} + [\boldsymbol{\mathcal{K}}' \cdot \mathbb{B}] \cdot \mathbb{B} + 2[\boldsymbol{\mathcal{C}}' \cdot \mathbb{B}] : \boldsymbol{F} \geqslant 0, \qquad \forall \boldsymbol{F} \in \mathcal{T},\ \forall \mathbb{B} \in \mathcal{V} \tag{2}$$

$$\left[\boldsymbol{\mathcal{A}}' : \boldsymbol{F}\right] : \boldsymbol{F} \geqslant 0, \qquad \forall \boldsymbol{F} \in \mathcal{T}, \tag{3}$$

$$[\boldsymbol{\mathcal{K}}' \cdot \mathbb{B}] \cdot \mathbb{B} \geqslant 0, \qquad \forall \mathbb{B} \in \mathcal{V}. \tag{4}$$

The conditions in Eqs. (3) and (4) imply that $\boldsymbol{\mathcal{A}}'$ and $\boldsymbol{\mathcal{K}}'$ are positive semi-definite. These conditions are intrinsically met because both of the tensors are derived from an appropriately chosen free energy function. In comparison to a linear spring, the convolution integral type potential function in Eq. (1) can be interpreted as the accumulation of an magneto-elastically stored energy while mechanical and magnetic stiffnesses as well as the mechanical deformation and the magnetic loading (induction) are continuously evolving. It is noteworthy to mention here that this potential function is a magneto-elastic extension of the energy potential proposed in our earlier works in the case of a purely mechanical curing, cf. (Hossain et al., 2009b). To derive the relations for these time-dependent stiffness tensors, a magneto-elastic coupled energy function is necessary which relates to the three magneto-elastic moduli tensors in the following way

$$\boldsymbol{\mathcal{A}}(t) = \frac{\partial^2 \Omega(t)}{\partial \boldsymbol{F} \partial \boldsymbol{F}}, \quad \boldsymbol{\mathcal{C}}(t) = \frac{\partial^2 \Omega(t)}{\partial \boldsymbol{F} \partial \mathbb{B}}, \quad \boldsymbol{\mathcal{K}}(t) = \frac{\partial^2 \Omega(t)}{\partial \mathbb{B} \partial \mathbb{B}}, \tag{5}$$

where $\Omega(t)$ is a coupled energy function for magneto-elastic polymers with time dependent material parameters. $\Omega(t)$ is nothing but an appropriate free energy that has been used for modelling a fully-cured magneto-sensitive polymer and is available in the literature (Otténio et al., 2008; Saxena and Ogden, 2011). The second law of thermodynamics in the form of the Clausius–Duhem inequality for an isothermal process can be written in the case of a magneto-elastic problem as

$$\boldsymbol{P} : \dot{\boldsymbol{F}} + \mathbb{H} \cdot \dot{\mathbb{B}} - \dot{\Phi} \geqslant 0, \tag{6}$$

where $\boldsymbol{P}, \mathbb{H}$ and Φ are the first Piola–Kirchhoff stress tensor, the magnetic field vector in the material configuration and the potential function from Eq. (1), respectively. In Eq. (6), $\dot{(\bullet)}$ is a material time derivative. To evaluate the above dissipation inequality, the

material time derivative of the energy potential Φ follows from adopting the Leibniz integral rule:

$$\begin{aligned}\dot{\Phi}(t) &= \frac{1}{2}\left[[\mathcal{A}'(s):[\boldsymbol{F}(t)-\boldsymbol{F}(s)]]:[\boldsymbol{F}(t)-\boldsymbol{F}(s)]\right]_{s=t}\\ &+\frac{1}{2}\int_0^t \frac{\partial}{\partial t}([\mathcal{A}'(s):[\boldsymbol{F}(t)-\boldsymbol{F}(s)]]:[\boldsymbol{F}(t)-\boldsymbol{F}(s)])ds\\ &+\frac{1}{2}[[\mathcal{K}'(s)\cdot[\mathbb{B}(t)-\mathbb{B}(s)]]\cdot[\mathbb{B}(t)-\mathbb{B}(s)]]_{s=t}\\ &+\frac{1}{2}\int_0^t \frac{\partial}{\partial t}([\mathcal{K}'(s)\cdot[\mathbb{B}(t)-\mathbb{B}(s)]]\cdot[\mathbb{B}(t)-\mathbb{B}(s)])ds\\ &+[[\mathcal{C}'(s)\cdot[\mathbb{B}(t)-\mathbb{B}(s)]]:[\boldsymbol{F}(t)-\boldsymbol{F}(s)]]_{s=t}\\ &+\int_0^t \frac{\partial}{\partial t}([\mathcal{C}'(s)\cdot[\mathbb{B}(t)-\mathbb{B}(s)]]:[\boldsymbol{F}(t)-\boldsymbol{F}(s)])ds\\ &=0+\frac{1}{2}\int_0^t[\mathcal{A}'(s):\dot{\boldsymbol{F}}(t)]:[\boldsymbol{F}(t)-\boldsymbol{F}(s)]ds\\ &+\frac{1}{2}\int_0^t[\mathcal{A}'(s):[\boldsymbol{F}(t)-\boldsymbol{F}(s)]]:\dot{\boldsymbol{F}}(t)ds+0\\ &+\frac{1}{2}\int_0^t[\mathcal{K}'(s)\cdot\dot{\mathbb{B}}(t)]\cdot[\mathbb{B}(t)-\mathbb{B}(s)]ds\\ &+\frac{1}{2}\int_0^t[\mathcal{K}'(s)\cdot[\mathbb{B}(t)-\mathbb{B}(s)]]\cdot\dot{\mathbb{B}}(t)ds+0\\ &+\int_0^t[\mathcal{C}'(s)\cdot\dot{\mathbb{B}}(t)]:[\boldsymbol{F}(t)-\boldsymbol{F}(s)]ds\\ &+\int_0^t[\mathcal{C}'(s)\cdot[\mathbb{B}(t)-\mathbb{B}(s)]]:\dot{\boldsymbol{F}}(t)ds\\ &=\left[\int_0^t\mathcal{A}'(s):[\boldsymbol{F}(t)-\boldsymbol{F}(s)]\right]:\dot{\boldsymbol{F}}(t)ds\\ &+\left[\int_0^t\mathcal{K}'(s)\cdot[\mathbb{B}(t)-\mathbb{B}(s)]\right]\cdot\dot{\mathbb{B}}(t)ds\\ &+\left[\int_0^t[\mathcal{C}'(s)\cdot[\mathbb{B}(t)-\mathbb{B}(s)]]\right]:\dot{\boldsymbol{F}}(t)ds\\ &+\left[\int_0^t[\mathcal{C}^{t'}(s):[\boldsymbol{F}(t)-\boldsymbol{F}(s)]]\right]\cdot\dot{\mathbb{B}}(t)ds.\end{aligned}\tag{7}$$

The last two equality signs in Eq. (7) require permutability of the double and single contractions, i.e.

$$[\mathcal{A}':\boldsymbol{B}]:\boldsymbol{C}=[\mathcal{A}':\boldsymbol{C}]:\boldsymbol{B}\quad\forall\boldsymbol{B},\boldsymbol{C}\in\mathcal{T}\Longleftrightarrow\quad(\mathcal{A}')_{ijkl}B_{kl}C_{ij}=(\mathcal{A}')_{klij}C_{ij}B_{kl},\tag{8}$$

and

$$[\mathcal{K}'\cdot\boldsymbol{a}]\cdot\boldsymbol{b}=[\mathcal{K}'\cdot\boldsymbol{b}]\cdot\boldsymbol{a}\quad\forall\boldsymbol{a},\ \boldsymbol{b}\in\mathcal{V}\Longleftrightarrow(\mathcal{K}')_{ij}a_jb_i=(\mathcal{K}')_{ji}b_ia_j,\tag{9}$$

which are given since $\mathcal{A}$ and $\mathcal{K}$ originate from potentials and thus possesses the required symmetries. Insertion of the result from Eq. (7) into the isothermal version of the second law of thermodynamics in Eq. (6) yields

$$\begin{aligned}&\left[\boldsymbol{P}(t)-\int_0^t[\mathcal{A}'(s):[\boldsymbol{F}(t)-\boldsymbol{F}(s)]]ds-\int_0^t[\mathcal{C}'(s)\cdot[\mathbb{B}(t)-\mathbb{B}(s)]]ds\right]:\dot{\boldsymbol{F}}(t)\\ &+\left[\mathbb{H}(t)-\int_0^t\left[\mathcal{C}^{t'}(s):[\boldsymbol{F}(t)-\boldsymbol{F}(s)]\right]ds\right.\\ &\left.-\int_0^t[\mathcal{K}'(s)\cdot[\mathbb{B}(t)-\mathbb{B}(s)]]ds\right]\cdot\dot{\mathbb{B}}(t)\geqslant 0,\end{aligned}\tag{10}$$

where $\mathcal{C}^t=\partial^2\Omega/\partial\mathbb{B}\partial\boldsymbol{F}$. In order to satisfy the above requirement for arbitrary values of $\dot{\boldsymbol{F}}$ and $\dot{\mathbb{B}}$, the following functionals result for the first Piola–Kirchhoff stress $\boldsymbol{P}$ and the magnetic field $\mathbb{H}$:

$$\boldsymbol{P}(t)=\int_0^t\mathcal{A}'(s):[\boldsymbol{F}(t)-\boldsymbol{F}(s)]ds+\int_0^t\mathcal{C}'(s)\cdot[\mathbb{B}(t)-\mathbb{B}(s)]ds,\tag{11}$$

and

$$\mathbb{H}(t)=\int_0^t\mathcal{C}^{t'}(s):[\boldsymbol{F}(t)-\boldsymbol{F}(s)]ds+\int_0^t[\mathcal{K}'(s)\cdot[\mathbb{B}(t)-\mathbb{B}(s)]]ds.\tag{12}$$

Such relations guarantee that the model is dissipation-free for arbitrary processes. To obtain more precise relations among stress, strain, magnetic field and magnetic induction, the Leibniz integral rule has to be applied once more that yields

$$\begin{aligned}\dot{\boldsymbol{P}}(t)&=\left[\mathcal{A}'(s):[\boldsymbol{F}(t)-\boldsymbol{F}(s)]\right]_{s=t}\\ &+\int_0^t\mathcal{A}'(s):\dot{\boldsymbol{F}}(t)ds+[\mathcal{C}'(s)\cdot[\mathbb{B}(t)-\mathbb{B}(s)]]_{s=t}\\ &+\int_0^t\mathcal{C}'(s)\cdot\dot{\mathbb{B}}(t)ds\\ &=\mathcal{A}(t):\dot{\boldsymbol{F}}(t)+\mathcal{C}(t)\cdot\dot{\mathbb{B}}(t),\end{aligned}\tag{13}$$

and

$$\begin{aligned}\dot{\mathbb{H}}(t)&=\left[\mathcal{C}^{t'}(s):[\boldsymbol{F}(t)-\boldsymbol{F}(s)]\right]_{s=t}\\ &+\int_0^t\mathcal{C}^{t'}(s):\dot{\boldsymbol{F}}(t)ds+[\mathcal{K}'(s)\cdot[\mathbb{B}(t)-\mathbb{B}(s)]]_{s=t}\\ &+\int_0^t\mathcal{K}'(s)\cdot\dot{\mathbb{B}}(t)ds\\ &=\mathcal{C}^t(t):\dot{\boldsymbol{F}}(t)+\mathcal{K}(t)\cdot\dot{\mathbb{B}}(t).\end{aligned}\tag{14}$$

Finally the evolutions of the stress and the magnetic field are given in rate forms as

$$\dot{\boldsymbol{P}}(t)=\mathcal{A}(t):\dot{\boldsymbol{F}}(t)+\mathcal{C}(t)\cdot\dot{\mathbb{B}}(t),\tag{15}$$

$$\dot{\mathbb{H}}(t)=\mathcal{C}^t(t):\dot{\boldsymbol{F}}(t)+\mathcal{K}(t)\cdot\dot{\mathbb{B}}(t).\tag{16}$$

The resulting Eqs. (15) and (16) are hypoelastic type relations for the stress and the magnetic field development during the curing process. Note that these relations inherit the physical observation that a curing material sustaining no current change of loadings (mechanical and magnetic) does not change its stress and magnetic field as resulted from previous deformations – even though its material properties continue to evolve. According to several papers (Atluri, 1984; Wriggers, 2008) hypoelastic constitutive relations may produce some physically unrealistic responses, e.g. stress hysteresis even in the case of elastic loading. We have tested our proposed formulations with some numerical examples that are illustrated in Appendix C. It is observed that no significant unphysical results are produced by the formulations. The stiffness tensors appearing in Eq. (5) will be obtained from the free energy function Ω which can be written in the indicial notation as

$$\begin{aligned}&\mathcal{A}_{\alpha i\beta j}(t)=\frac{\partial^2\Omega(t)}{\partial F_{i\alpha}\partial F_{j\beta}},\quad \mathcal{C}_{\alpha i\beta}(t)=\frac{\partial^2\Omega(t)}{\partial F_{i\alpha}\partial B_\beta},\\ &\mathcal{C}^t_{\beta i\alpha}(t)=\frac{\partial^2\Omega(t)}{\partial B_\beta\partial F_{i\alpha}},\quad \mathcal{K}_{\alpha\beta}(t)=\frac{\partial^2\Omega(t)}{\partial B_\alpha\partial B_\beta}.\end{aligned}\tag{17}$$

Note that the magneto-elastic moduli tensors $\mathcal{A}$ and $\mathcal{K}$ have minor symmetry, i.e. $\mathcal{A}_{\alpha i\beta j}=\mathcal{A}_{\beta j\alpha i}$ and $\mathcal{K}_{\alpha\beta}=\mathcal{K}_{\beta\alpha}$ but the coupled tensor $\mathcal{C}$ has no indicial symmetry. To determine the above-mentioned three stiffness moduli, we need an energy function which is commonly used for modelling particle-filled fully-cured magneto-elastic polymers.

Consider a situation in which the material has a preferred direction due to an alignment of the ferromagnetic particles. Let the direction is given in the reference configuration by a unit vector **a**. On application of a magnetic induction $\mathbb{B}$, there are in effect two preferred directions. For such a material, the energy density function $\Omega=\tilde{\Omega}(\boldsymbol{F},\mathbb{B},\mathbf{a})$ can be specified in the form of ten linearly independent scalar invariants, cf. Spencer, 1971 and Bustamante, 2010. In our case, we choose the invariants to be

$$I_1 = \mathrm{tr}\boldsymbol{C}, \quad I_2 = \frac{1}{2}\left[I_1^2 - \mathrm{tr}\boldsymbol{C}^2\right], \quad I_3 = \det \boldsymbol{C}, \quad I_4 = \mathbb{B}\cdot\mathbb{B},$$
$$I_5 = \mathbb{B}\cdot[\boldsymbol{C}\mathbb{B}], \quad I_6 = [\boldsymbol{C}\mathbb{B}]\cdot[\boldsymbol{C}\mathbb{B}], \quad I_7 = \mathbf{a}\cdot[\boldsymbol{C}\mathbf{a}], \quad I_8 = [\boldsymbol{C}\mathbf{a}]\cdot[\boldsymbol{C}\mathbf{a}],$$
$$I_9 = \mathbf{a}\cdot\mathbb{B}, \quad I_{10} = \mathbf{a}\cdot[\boldsymbol{C}\mathbb{B}], \tag{18}$$

where $\boldsymbol{C} = \boldsymbol{F}^t\boldsymbol{F}$ is the right Cauchy-Green strain tensor.

However, in the case of curing of a magnetoelastic polymer under the presence of a magnetic induction, the alignment of the ferromagnetic particles always occurs in the direction of an externally applied magnetic induction, cf. Fig. (2). Thus, the magnetic induction can be written as a scalar multiple of the preferred direction, i.e. $\mathbb{B} = \beta\mathbf{a}$. For this simplification, we obtain the following relations

$$I_4 = \beta I_9 = I_9^2, \quad I_5 = I_9^2 I_7 = I_9 I_{10}, \quad I_6 = I_4 I_8. \tag{19}$$

Hence, the only linearly independent invariants are $I_1,\ldots,I_6$ and henceforth we consider the energy density to be dependent only on them, i.e. for an unconstrained isotropic material, Ω is a function of the invariants $I_1, I_2, I_3, I_4, I_5, I_6$. Therefore, expressions for the three different time-dependent stiffness tensors defined in Eq. (5) can be expanded in the form below

$$\mathcal{A}_{\alpha i\beta j}(t) = \sum_{\zeta=1,\,\zeta\neq4}^{6}\sum_{\eta=1,\,\eta\neq4}^{6}\Omega_{\zeta\eta}(t)\frac{\partial I_\eta}{\partial F_{i\alpha}}\frac{\partial I_\zeta}{\partial F_{j\beta}} + \sum_{\eta=1,\eta\neq4}^{6}\Omega_\eta(t)\frac{\partial^2 I_\eta}{\partial F_{i\alpha}\partial F_{j\beta}} \tag{20}$$

$$\mathcal{C}_{\alpha i\beta}(t) = \sum_{\zeta=4}^{6}\sum_{\eta=1,\,\eta\neq4}^{6}\Omega_{\zeta\eta}(t)\frac{\partial I_\zeta}{\partial B_\beta}\frac{\partial I_\eta}{\partial F_{i\alpha}} + \sum_{\eta=5}^{6}\Omega_\eta(t)\frac{\partial^2 I_\eta}{\partial F_{i\alpha}\partial B_\beta} \tag{21}$$

$$\mathcal{K}_{\alpha\beta}(t) = \sum_{\zeta=4}^{6}\sum_{\eta=4}^{6}\Omega_{\zeta\eta}(t)\frac{\partial I_\zeta}{\partial B_\alpha}\frac{\partial I_\eta}{\partial B_\beta} + \sum_{\eta=4}^{6}\Omega_\eta(t)\frac{\partial^2 I_\eta}{\partial B_\alpha\partial B_\beta} \tag{22}$$

where $\Omega_\eta(t) = \partial\Omega(t)/\partial I_\eta, \Omega_{\zeta\eta}(t) = \partial^2\Omega(t)/\partial I_\zeta\partial I_\eta$. Expressions for the first and second order derivatives of $I_\eta(\eta = 1,\ldots,6)$ with respect to $\boldsymbol{F}$ and $\mathbb{B}$ are given in the Appendix A. In the following sections, the framework for the simulation of magneto-elastic curing materials described above will be specialised for a phenomenologically-motivated Mooney–Rivlin type free energy function. To this end, expressions for the coefficients $\Omega_\eta, \Omega_{\zeta\eta}$ that are required for the three different elastic tangent moduli, i.e. $\mathcal{A}, \mathcal{K}$ and $\mathcal{C}$ are derived.

3. Application to curing of magneto-sensitive polymers

A magneto-elastic energy function can be obtained following the framework of the compressible Mooney–Rivlin model. This is a slight generalisation of a Mooney–Rivlin type magnetoelastic energy function proposed by Otténio et al. (2008). The energy function with various time-dependent material parameters is

$$\Omega(t) = \frac{\mu(t)}{4}\left[1 + \alpha_e\tanh\left(\frac{I_4}{m_e}\right)\right][[1+n][I_1-3] + [1-n][I_2-3]] + \frac{1}{8}\kappa(t)[\ln I_3]^2 - \frac{1}{2}\mu(t)\ln I_3 + l(t)I_4 + m(t)I_5 \tag{23}$$

where $\mu(t), \kappa(t)$ are time-dependent mechanical parameters while $l(t)$ and $m(t)$ are coupling parameters. The rest of the parameters, e.g. α_e, n, are some scaling constants. The invariants I_1, I_2, I_3, I_4, I_5 are already defined in Eq. (18). Note that in contrast to the classical Mooney–Rivlin energy function, here additional terms are introduced to take account for the compressibility of the material. In Eq. (23), $\mu(t)$ is the shear modulus of the material in the absence of a magnetic field and n is a dimensionless parameter within the range $-1 \leqslant n \leqslant 1$, as for the classical Mooney–Rivlin model. The additional term $[1 + \alpha_e\tanh(I_4/m_e)]$ corresponds to an increase in the stiffness due to the magnetisation and the phenomenon of magnetic saturation after a critical value of magnetisation. The parameter m_e is required for the purpose of non-dimensionalisation while α_e is a dimensionless positive parameter for scaling. The magneto-elastic coupling parameters $l(t)$ and $m(t)$ have the dimensions of μ_0^{-1}, μ_0 being the magnetic permeability of vacuum. For $\alpha_e = l = m = 0$, this simplifies to the compressible Mooney–Rivlin elastic energy density function widely used to model compressible elastomers. In order to derive the various magneto-elastic moduli tensors described in Eqs. (20)–(22), the scalar-valued coefficients $\Omega_\eta(t)$ and $\Omega_{\zeta\eta}(t)$ have to be derived. For the above chosen energy function, the non-zero coefficients are,

$$\Omega_1 = \frac{\mu}{4}\left[1 + \alpha_e\tanh\left(\frac{I_4}{m_e}\right)\right][1+n],$$

$$\Omega_2 = \frac{\mu}{4}\left[1 + \alpha_e\tanh\left(\frac{I_4}{m_e}\right)\right][1-n],$$

$$\Omega_3 = \frac{\kappa}{4I_3}\ln I_3 - \frac{\mu}{2I_3}, \quad \Omega_5 = m,$$

$$\Omega_4 = l + \frac{\mu\alpha_e}{4m_e}\left[1 - \tanh^2\left(\frac{I_4}{m_e}\right)\right][[1+n][I_1-3] + [1-n][I_2-3]],$$

$$\Omega_{14} = \frac{\mu\alpha_e}{4m_e}\left[1 - \tanh^2\left(\frac{I_4}{m_e}\right)\right][1+n],$$

$$\Omega_{33} = \frac{\kappa}{4I_3^2} - \frac{\kappa}{4I_3^2}\ln I_3 + \frac{\mu}{2I_3^2},$$

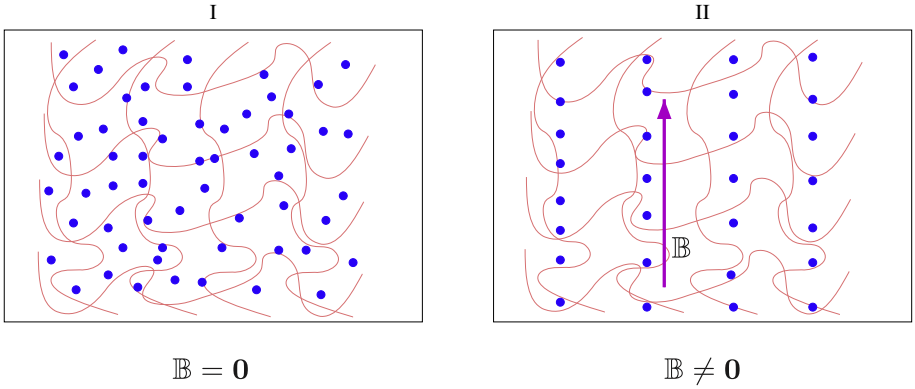

Fig. 2. Particles alignment during curing: (I) in the absence of a magnetic induction, isotropic material; (II) preferred direction in the presence of a magnetic induction.

$$\Omega_{44} = -\frac{\mu\alpha_e}{2m_e^2}\left[\tanh\left(\frac{I_4}{m_e}\right)\left[1-\tanh^2\left(\frac{I_4}{m_e}\right)\right]\right] [[1+n][I_1-3]+[1-n][I_2-3]],$$

$$\Omega_{24} = \frac{\mu\alpha_e}{4m_e}\left[1-\tanh^2\left(\frac{I_4}{m_e}\right)\right][1-n].$$

Note that the remaining coefficients required in Eqs. (20)–(22) are simply zero. Once relevant coefficients are determined, the three stiffness moduli required in Eqs. (15) and (16) are calculated with the help of the expressions presented in the Appendix A.

4. Parameters evolution during curing

Several material parameters have appeared in the proposed model. The number of the material parameters depends on the choice of the free energy function required for the derivation of the three time-dependent stiffness moduli. Some parameters relate to the pure mechanical part of the energy function while few of them are related with its coupled part. As in the case of purely mechanical curing, we make arbitrary but reasonable choices for modelling the temporal evolution of the material parameters due to the lack of sufficient experimental data. One of the easiest formats for the evolving parameters can be an exponential saturation function as

$$x(t) = x_0 + [x_\infty - x_0]\left[1-\exp(-\kappa_p t)\right], \tag{24}$$

being governed by the initial and the final values x_0 and x_∞, respectively, as well as the curvature parameter κ_p. In the case of the shear modulus evolution, the initial and final cut-off values, i.e. x_0 and x_∞, respectively, are replaced by μ_0 and μ_∞ while the curvature parameter κ_p is substituted by κ_μ. A specification of (24) is plotted in Fig. (3) in the case of the shear modulus evolution. For the sake of simplicity, the elastic bulk modulus is calculated using a relationship that is commonly used in polymeric material modelling, i.e. the ratio of the shear modulus to the bulk modulus. In this case, we take the ratio as $\mu/\kappa = 0.1$ which is close to a poisson's number of $\nu = 0.45$ in the case of small deformations.

According to several papers (Chen et al., 2007; Xu et al., 2011), the coupled magneto-mechanical parameters may evolve following the format of an exponential saturation function. There are two coupled parameters, i.e. $m(t)$ and $l(t)$, appearing in the chosen energy function. We take a similar approach as in the case of the mechanical material parameters for parameter $m(t)$ evolution, i.e. an exponential saturation function as in Eq. (24). In this case, the two cut-off values, i.e. x_0 and x_∞ are replaced by m_0 and m_∞, respectively, while the curvature parameter κ_p is substituted by κ_m. However, the other parameter $l(t)$ is taken as a constant in all simulations presented in Section (5).

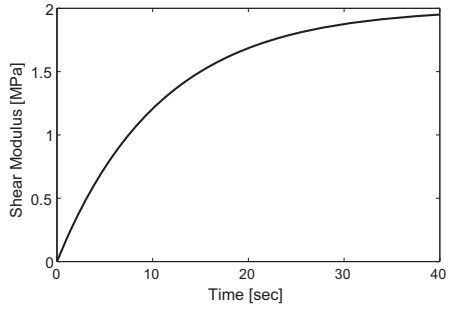

Fig. 3. Evolution of the shear modulus $\mu(t)$ with $[\mu_0, \mu_\infty, \kappa_\mu] = [0.0001\ \text{N/m}^2, 2.0\ \text{N/m}^2, 0.0925\ \text{s}^{-1}]$.

5. Numerical examples

Discretizing the relations in Eqs. (15) and (16) with an Euler-backward type implicit integrator, we obtain

$$\boldsymbol{P}^{i+1} = \boldsymbol{P}^i + \boldsymbol{\mathcal{A}}^{i+1} : [\boldsymbol{F}^{i+1} - \boldsymbol{F}^i] + \boldsymbol{\mathcal{C}}^{i+1} \cdot [\mathbb{B}^{i+1} - \mathbb{B}^i], \tag{25}$$

and

$$\mathbb{H}^{i+1} = \mathbb{H}^i + \boldsymbol{\mathcal{C}}^{t,i+1} : [\boldsymbol{F}^{i+1} - \boldsymbol{F}^i] + \boldsymbol{\mathcal{K}}^{i+1} \cdot [\mathbb{B}^{i+1} - \mathbb{B}^i], \tag{26}$$

where $[\bullet]^i = [\bullet](t_i), t_{i+1} = t_i + \Delta t$ and Δt is a time step. For the case of mechanical loading, the deformation gradient $\boldsymbol{F}$ is the input while the magnetic induction vector $\mathbb{B}$ is the same for the magnetic loading. The actual stiffness moduli $\boldsymbol{\mathcal{A}}^{i+1}, \boldsymbol{\mathcal{C}}^{i+1}$ and $\boldsymbol{\mathcal{K}}^{i+1}$ need to be calculated using expressions (20)–(22) with the help of a Mooney–Rivlin type energy function given in Eq. (23). In the first part of this section, all of the tests presented are of uniaxial type while in the second part, a shear mode test is examined with various loading options. For the uniaxial tests, the constitutive model discussed above needs to be formulated in one-dimensional form. As per the definition of a uniaxial tension test, the specimen is elongated only in one direction, i.e. $\lambda_1 = \lambda$, while the other two lateral directions are free to move. In a three-dimensional setting, the complete deformation gradient ($\boldsymbol{F}$) reads

$$\boldsymbol{F} = \begin{bmatrix} \lambda_1 & 0 & 0 \\ 0 & \lambda_2 & 0 \\ 0 & 0 & \lambda_3 \end{bmatrix} \tag{27}$$

and the magnetic induction vector ($\mathbb{B}$) is

$$\mathbb{B} = \begin{bmatrix} B_1 \\ 0 \\ 0 \end{bmatrix}. \tag{28}$$

Now one of the important tasks is to establish a relation between λ_1 and λ_2 ($\lambda_2 = \lambda_3$ in the case of symmetric deformation) in the case of a compressible material as assumed in the current study. Note that since the elongation is only in one direction, the specimen will contract in the transversal directions and due to the stress-free boundary conditions, both nominal stresses P_{22} and P_{33} are zero and only the nominal stress P_{11} needs to be determined. For a relation between λ_1 and λ_2 in the case of a uniaxial mode, detailed derivations are presented in Appendix B. In this section, three different types of numerical experiments are performed to obtain the corresponding solutions. The following numerical values of the material parameters are used unless otherwise stated to have a different value for individual computation

$$\alpha_e = 1, \quad m_e = 1\ \text{T}^2, \quad n = 0.5, \quad \mu/\kappa = 0.1. \tag{29}$$

5.1. Uniaxial tension tests

5.1.1. Example type I

With an aim to check whether the proposed finite strain curing model will predict the gain in the stiffness during the advancement of curing and provide a correct behaviour in the case when the mechanical strain rate becomes zero and/or the magnetic induction rate is zero, at first a simple uniaxial tension numerical test is performed. To this end a three phase deformation for the case of the mechanical loading, i.e. *pull-hold-pull* is applied consisting of a linear increase of the stretch to $\lambda = 1.25$ within the first twenty seconds which is followed by hundred sixty seconds holding and another linear increase of the stretch to $\lambda = 1.5$ during the last twenty seconds, cf. Fig. (4, left). Such mechanical loading history is applied in both cases (Case I and II, see Fig. 4) while in the first case, in combination with the mechanical loading, the simulation

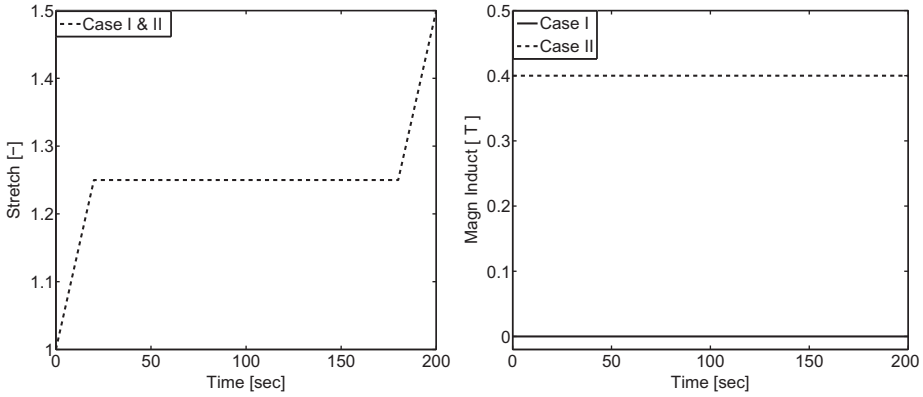

Fig. 4. Example type I: three-steps mechanical load history in Case I and II (left); a zero and a constant magnetic inductions are applied in both cases, respectively (right).

is performed in the absence of a magnetic induction (in purely mechanical loading, $B_1 = 0.0$) and in the second case, the simulation is run by a constant magnetic induction of magnitude 0.4 T, i.e. $B_1 = 0.4$ T, cf. Fig. (4, right).

For both loading cases, an exponential saturation function for the evolution of the shear modulus $\mu(t)$ and also for the coupled parameter $m(t)$ are used as depicted in Fig. (3). Note that the shape of the exponential saturation functions for the mechanical shear modulus evolution and the coupled parameter evolution are qualitatively the same but their initial and final saturation points and curvature parameters are different. The resulting total stress response versus time is plotted in Fig. (5, left) while the magnetic field versus curing time is depicted in Fig. (5, right). With the three-phase mechanical loading, the physical observation upon which the constitutive model is formulated is verified. This implies that the stiffness increase during curing has no impact on the stress response of a constant mechanical deformation state is correctly reproduced in the absence of a magnetic load ($\mathbb{B} = \boldsymbol{0}$), which is reflected by the constant line of the mechanical stress between 21 and 180 s, cf. Fig. (5, left). Moreover, the kinks at $\lambda = 1.25$ in Fig. (6) illustrate the same argument. The initially fast growing shear modulus leads to a nonlinear stress growth during the first twenty seconds, whereas the behaviour is almost linear with a high stiffness at the end since the saturation value for the shear modulus $\mu(t)$ has been reached meanwhile, cf. Fig. (3). The stiffness gain that comes from the modulus $\mathcal{A}$ is more vivid when we plot the total stress over the mechanical stretch, see Fig. (6, left). Similarly, the stiffness gain due to the modulus $\mathcal{C}$ is depicted if we plot the magnetic field over the mechanical stretch, see Fig. (6, right). It can be noted here that a constant amount of magnetic induction with a mechanical load, in comparison to a simulation without a magnetic induction, increases the stress response and the stiffness as depicted in Figs. (5, left) and (6), respectively. In addition to the material parameters listed in Eq. (29), more parameters used for this simulation are in Table 1.

5.1.2. Example type II

To check the influence of the mechanical and magnetic loadings simultaneously, another simple uniaxial tension example is performed. This set of numerical tests will also predict the gain in the stiffness during the advancement of curing as well as coupled response due to a magneto-mechanical loading. Here, similar to the previous step-wise loading, a three phase magnetic loading, i.e. *pull-hold-pull* is applied that consists of a linear increase of the magnetic induction to $B_1 = 0.2$ T within the first twenty seconds which is followed by hundred sixty seconds holding and another linear increase of the induction to $B_1 = 0.2$ T during the last twenty seconds, cf. Fig. (7, right). Such magnetic loading history is applied in both cases (Case I and II, cf. Fig. 7) while in the first case the simulation is run in the absence of a mechanical loading (in purely magnetic loading, $\lambda_1 = \lambda_2 = \lambda_3 = 1.0$). In the second case, in combination with the three-phase magnetic loading, the numerical test is performed by a constant mechanical stretch of 1.5, i.e. $\lambda = 1.5$, cf. Fig. (7, left).

Similar to the first numerical tests, an exponential saturation function for the evolution of the shear modulus $\mu(t)$ and also for the coupled parameter $m(t)$ are used as depicted in Fig. (3). The total nominal stress versus time for the above mentioned loading history is depicted in Fig. (8, left) while the measured magnetic field versus curing time is depicted in Fig. (8, right). The physical observation that the stiffness increases during curing has no impact on the stress response of a constant deformation state is correctly reproduced in the case of the magnetic loading also. This fact is implied by the constant lines for the stress and magnetic field responses between 21 and 180 s, cf. Figs. (8, left) and (8, right). The concept of stiffness gains can be vivid when the plots for the stress and the magnetic field are illustrated over the mechanical stretch and the magnetic induction, respectively. The kinks in Fig. (9) for the magnetic induction at $\mathbb{B}_1 = 0.2$ T are due to the continuous increase of the shear modulus $\mu(t)$ as well as the magnetic coupled parameter $m(t)$. We can see here that the stiffness gain, cf. Fig. (8, right) in the case of the second load (181–200 s) is not too high in comparison to the first load case since we take a constant value for the coupled material parameter l. The increment of the stiffness occurs only due to the effect of the coupled-magnetic parameter $m(t)$ which evolves in the same fashion as in the case of the mechanical shear modulus. It is noted that a constant amount of the mechanical loading ($\lambda = 1.5$), in comparison to a simulation without a mechanical loading, increases the stress and the magnetic field responses as depicted in Figs. (8) and (9), respectively. The difference between a simulation without a mechanical loading (in purely magnetic case, $\lambda_1 = \lambda_2 = \lambda_3 = 1.0$) and a simulation without a magnetic loading (in purely mechanical case, $\mathbb{B} = \boldsymbol{0}$) is that the magnetic loading is producing a stress response in the absence of a mechanical load while there is an insignificant magnetic field in the absence of a magnetic induction even with a mechanical load. Therefore, we can conclude that all relevant phenomena during the curing process that are observed with coupled as well as individual loadings are correctly captured by this novel constitutive model. Material parameters used for this simulation are the same as in the Example type I.

5.1.3. Example type III

A third type of numerical examples is presented within this section to demonstrate that the proposed model is appropriate to correctly reproduce relevant behaviours with a magneto-mechanical coupled loading. In load Case I, a three-step mechanical load,

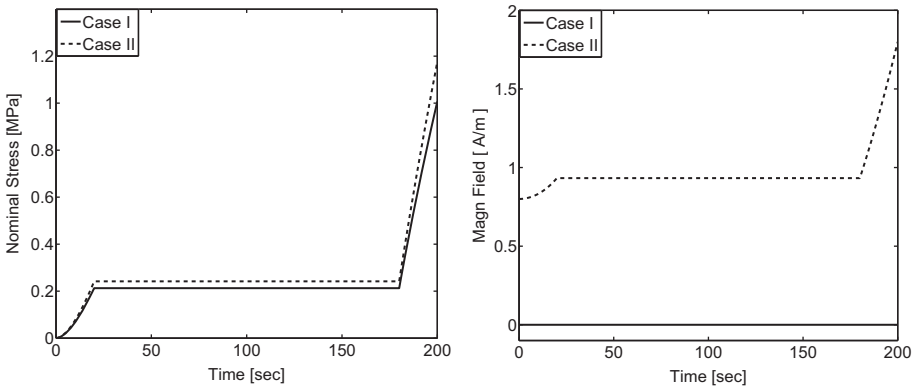

Fig. 5. Example type I: (Left) evolution of total stress with (dotted line) and without magnetic load (solid line); (Right) change of magnetic field H_1 (H_1 being a component of the magnetic field vector $\mathbb{H}$ in the x_1 direction) for a step-wise mechanical loading without a magnetic induction B_1 (solid line, no response for a zero magnetic induction) and in combination of a constant magnetic induction (dotted line).

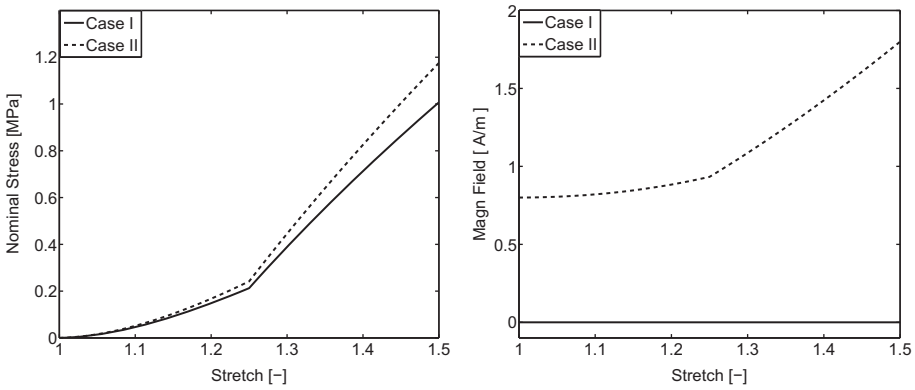

Fig. 6. Example type I: (Left) total nominal stress vs mechanical strain: presence of a constant magnetic loading increases total stiffness as well as mechanical stiffness from $\mathcal{A}$ is increasing in the case of the continuous curing; (Right) magnetic field vs mechanical stretch represents magnetic stiffness gain that originates from $\mathcal{C}$ in the presence of a constant magnetic induction.

Table 1
Baseline values of the material parameters for Example type I.

μ_0 [MPa]	μ_∞ [MPa]	m_0 [A^2/N]	m_∞ [A^2/N]	κ_μ/κ_m [s^{-1}]	l [A^2/N]
10^{-4}	2.0	10^{-4}	1.0	0.0225	1

i.e. *pull-hold-pull* is applied while a linearly increasing induction is applied for the magnetic case, see Fig. (10, solid lines). For the load Case II, a linearly increasing load is applied for the mechanical case while a three-step magnetic induction, i.e. *pull-hold-pull* is applied for the magnetic case, cf. Fig. (10, dotted lines). Similar to the previous examples, an exponential saturation function for the evolution of the shear modulus $\mu(t)$ and the coupled parameter $m(t)$ are used as depicted in Fig. (3). As mentioned in the previous section, the current bulk modulus has always been calculated from the shear modulus to the bulk modulus ratio of $\mu/\kappa = 0.1$.

In Case III, for the three-phase mechanical deformation, a linear increase of the stretch to $\lambda = 1.25$ within the first twenty seconds which is followed by hundred sixty seconds holding and another linear increase to $\lambda = 1.5$ during the last twenty seconds,

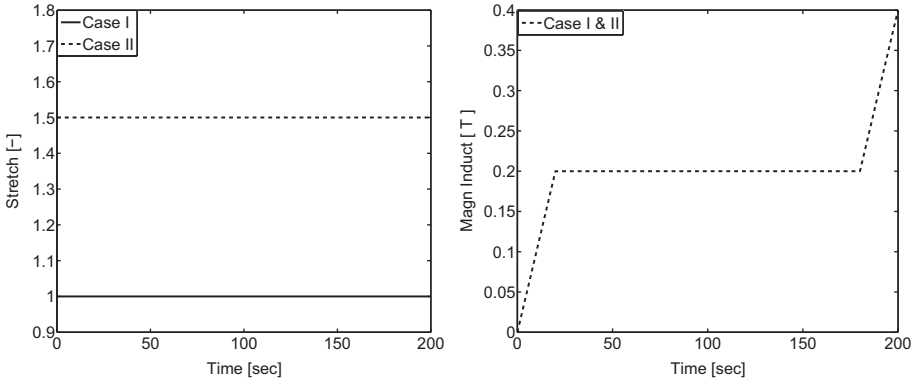

Fig. 7. Example type II: Three-steps magnetic load history in Case I and II (right); a zero and a constant mechanical stretches in both cases, respectively (left).

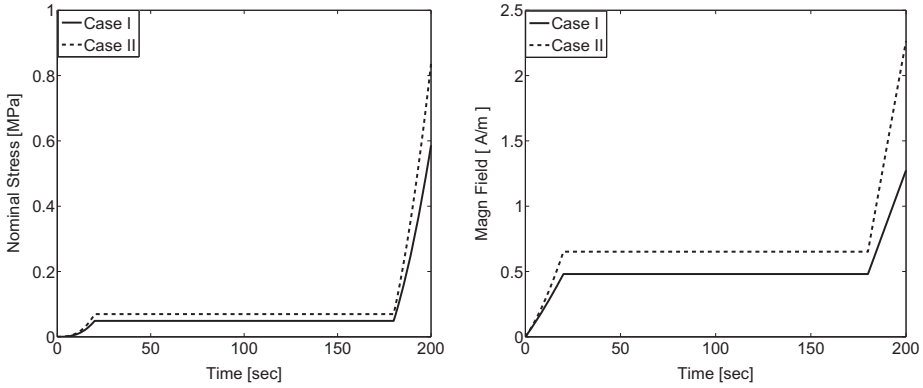

Fig. 8. Example type II: (Left) evolution of total stress for a step-wise magnetic load (solid line); (Right) change of magnetic field H_1 for a step-wise magnetic induction B_1 but no mechanical loading (solid line, no response for mechanical load) and in combination with a constant mechanical stretch (dotted line).

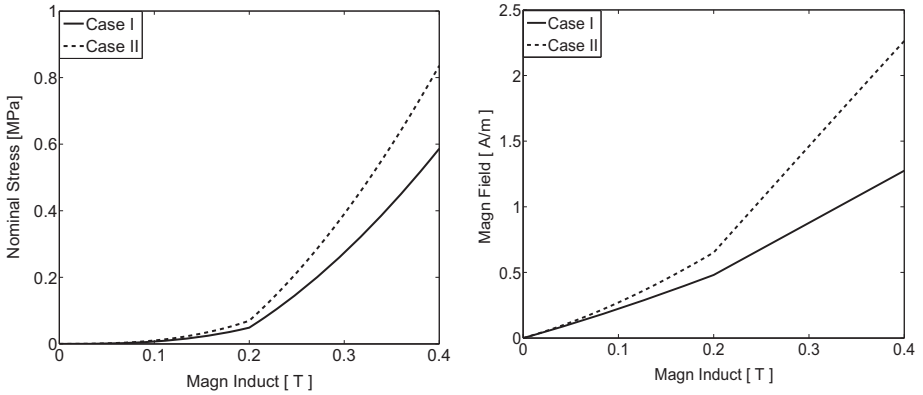

Fig. 9. Example Type II: (Left) total stress vs magnetic strain highlight stiffness gain from $\mathcal{C}$ during curing; (Right) magnetic field over magnetic induction presents magnetic stiffness gain that comes from $\mathcal{K}$ where stiffness gain is not higher in the second load increment as compared to the mechanical case.

cf. Fig. (10). This mechanical loading is combined with a linearly increasing magnetic load of a constant slope of 2.0×10^{-4} T s^{-1}. The stress response for the three-phase mechanical loading is similar in comparison to a three-phase mechanical loading with a magnetic load but here a linearly increasing magnetic load is responsible for an increment of the stress between the time period of the plateau, i.e. 21–180 s, cf. Fig. (11, left). That means, if there is no increment of the mechanical loading but a constant increment of the magnetic load, it still yields an increment in the total stress. Similarly, a three-phase magnetic loading with a mechanical stretch of constant slope of 0.0025 s^{-1} between the time period of the plateau, i.e. 21–180 s, will yield a magnetic field increment, cf. Fig. (11, right). It is noted here that in the case of the magnetic field response, cf. Fig. (11, right), the increment of the magnetic field in the second load case is larger than the first load case since in both coupling cases, a mechanical stretch is present. Therefore, the shear modulus is coupled with the parameter $m(t)$ which is responsible for a faster response in the second load case. In addition to the material parameters listed in Eq. (29), few more parameters used for these simulations are in Table 2.

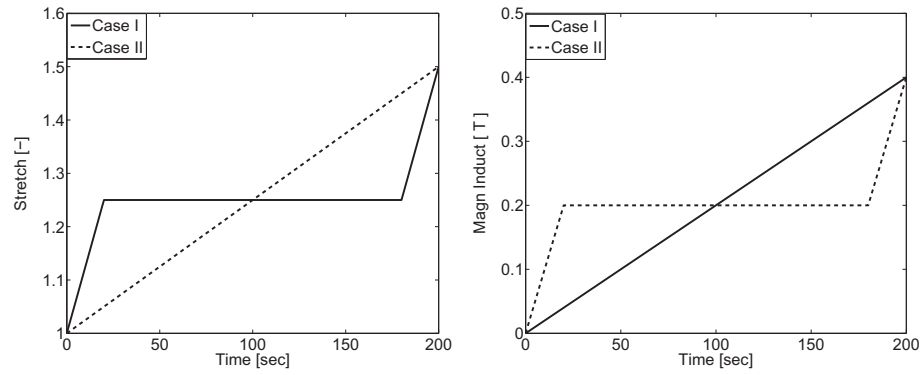

Fig. 10. Example type III: a three-step and a linearly increasing mechanical load history in Case I and II (left), respectively while a three-step and a linearly increasing magnetic induction applied in Case I and II (right), respectively.

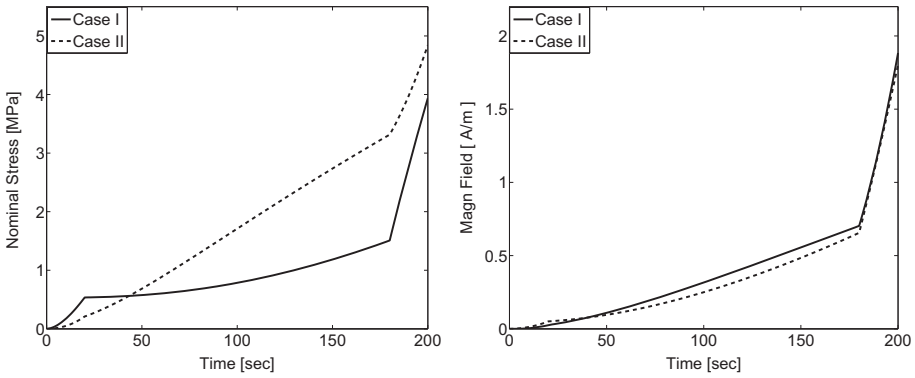

Fig. 11. Example type III: (Left) evolution of total nominal stress over time where an incremental magnetic load increases the total stress despite the fact that there is no mechanical load increment in the plateau over curing time; (Right) change of magnetic field H_1 for a step-wise mechanical loading with an incremental magnetic induction B_1 (solid line) and for a step-wise magnetic loading with an incremental mechanical stretch (dotted line).

Table 2
Baseline values of the material parameters for Example type III.

μ_0 [MPa]	μ_∞ [MPa]	m_0 [A^2/N]	m_∞ [A^2/N]	κ_μ/κ_m [s^1]	l [A^2/N]
10^{-4}	5.0	10^{-4}	0.5	0.0225	10^{-7}

5.2. Shear tests

In this section, we present few examples for a shear-type load only. The mechanical shear load is applied in x_1-x_2 plane. For such a deformation mode, in a three-dimensional setting, the complete deformation gradient is $\boldsymbol{F} = \boldsymbol{e}_1 \otimes \boldsymbol{e}_1 + \boldsymbol{e}_2 \otimes \boldsymbol{e}_2 + \gamma \boldsymbol{e}_1 \otimes \boldsymbol{e}_2 + \boldsymbol{e}_3 \otimes \boldsymbol{e}_3$, where γ is the amount of shear and $\boldsymbol{e}_i (i = 1, 2, 3)$ are the orthonormal unit vectors. Note that the above definition of a simple shear is an isochoric deformation where a plane strain ($F_{33} = 1$) condition is considered. This widely used definition can be denoted as an *incompressible plane strain definition of the simple shear* where a plane stress condition is applied, cf. Destrade et al. (2012). We denote it as the version I. However, the material, which we are working with, is a compressible one. Therefore, we take another definition of the shear mode where the complete deformation gradient is $\boldsymbol{F} = \boldsymbol{e}_1 \otimes \boldsymbol{e}_1 + \boldsymbol{e}_2 \otimes \boldsymbol{e}_2 + \gamma \boldsymbol{e}_1 \otimes \boldsymbol{e}_2 + \lambda \boldsymbol{e}_3 \otimes \boldsymbol{e}_3$. Here γ is the amount of shear and λ is a stretch in the out of plane direction. This definition can be termed as a *compressible plane stress ($P_{33} = 0$) definition of the simple shear* where $\sqrt{I_3} = \det \boldsymbol{F} \neq 1$. We denote it as the version II. For such a case, the unknown stretch λ in the out of plane direction has to be calculated iteratively from a given value of shear stretch γ considering $P_{33} = 0$. A recipe for such an iterative procedure is described in Appendix B for a uniaxial load case.

The magnitude of the shear is varied with the curing time in two ways, (i) a three-phase shear load, i.e. pull-hold-pull and (ii) a linearly increasing shear load. For all cases, a two hundred second time span is considered where the rate parameter κ_μ appearing in Eq. (24) is 0.0225 s^{-1}. In addition to the parameters listed in Eq. (29), the tabular parameters from Table 1 are also taken in this simulation. At first, we compare the two versions of shear modes for both load cases. Along with the three-step shear load, a three phase magnetic load is also applied in the x_1 direction ($B_1 \neq 0$) and the corresponding shear stress P_{12} is plotted in Fig. 12 (left, three-phase load) while a linearly increasing mechanical and a linearly increasing magnetic load are applied in the x_1 direction and results are presented in Fig. 12 (right, linearly increasing load). We apply the linearly increasing mechanical and magnetic load simultaneously with the same span of time, i.e. 200 s. The slope of the mechanical and magnetic loads are 10^{-3} s^{-1} and 0.005 T s^{-1}, respectively. In both load cases, the *compressible plane stress ($P_{33} = 0$) definition of the simple shear* yields a large stress compared to the *incompressible plane strain definition of the simple shear*. This difference, though very small in magnitude, is expected since in the case of compressible version of the simple shear, a small amount of volumetric stress is added to the total stress value that is depicted clearly in Fig. 12 (dotted lines). Such a comparison

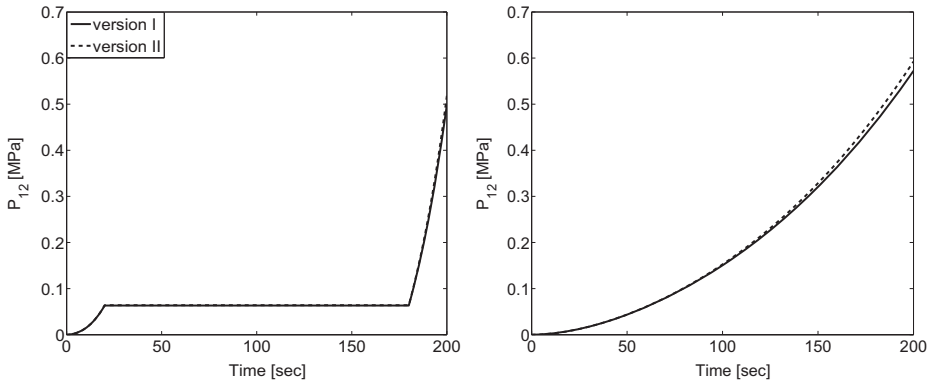

Fig. 12. Evolution of total shear stress over curing time; (Left) a three-phase magneto-mechanical coupled load is applied when the magnetic induction is in the x_1 direction (version I, solid line; version II, dotted line). (Right) a linearly increasing magneto-mechanical coupled load is applied when the magnetic induction is in the x_1 direction (version I, solid line; version II, dotted line).

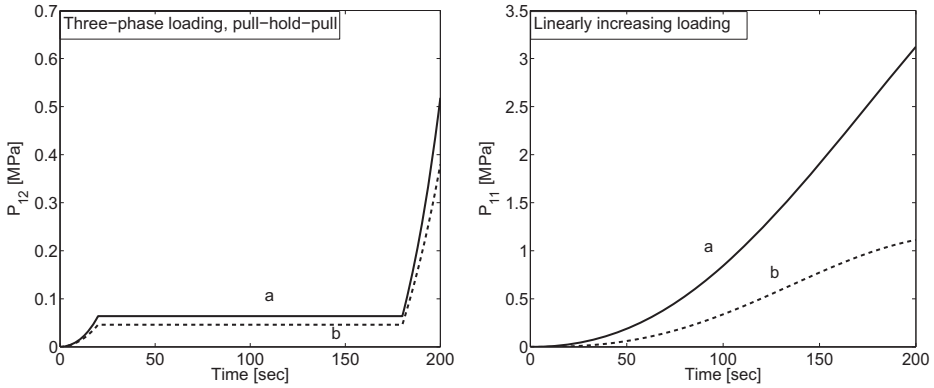

Fig. 13. (Left) evolution of total shear stress over curing time when a three-phase magneto-mechanical coupled load is applied in the x_1 direction (a, solid line) and in the x_2 direction (b, dotted line). (Right) evolution of total normal stress over curing time when a linearly increasing magneto-mechanical coupled load is applied in the x_1 direction (a, solid line) and in the x_2 direction (b, dotted line).

is more vivid in the case of a linearly increasing load, cf. Fig. 12 (right).

If we apply the three phase magnetic load in the x_2 direction ($B_2 \neq 0$), the total shear stress P_{12} will be less than the previous case, cf. Fig. 13 (left, b). Note that in the case of shear mode with a pull-hold-pull load, the basic assumptions that are inherited in the model are again verified, i.e. the stiffness gaining during curing and the chains are formed in an unstrained state. The amount of shear stress in the third load phase (181–200 s) is relatively higher than in the first load phase (0–20 s) due to a stiffness gaining within the holding period of 21–180 s. In this case and the example follows, the compressible version of the deformation gradient is taken.

A time-dependent variation of the normal stresses can also be demonstrated. The normal stress P_{11} shows a strong coupling with the applied magnetic load. For the linearly increasing load, the normal stress P_{11} is plotted. When the magnetic induction is applied in the x_1 direction, it enhances the total stress, i.e. Fig. 13 (right, a) compared to the situation when it is applied in the x_2 direction, cf. Fig. 13 (right, b). A similar behaviour can be observed for the normal stress P_{22}. For all simulations presented in this section, the evolution of the coupled parameters $m(t)$ is considered as an exponential saturation function qualitatively depicted in Fig. (3). For all other material parameters used in these simulations, see Eq. (29) and Table 1.

6. Conclusion and outlook

In this contribution, we propose a three-dimensional, thermodynamically consistent framework for the simulation of polymeric materials undergoing curing processes in the case of a magneto-mechanical coupled finite deformation. Starting from the idea of continuous chain crosslinking that is conceptualized by the addition of more and more springs, a convolution integral type potential function is proposed. Such potential function represents accumulation of a magnetoelastic stored energy that yields, after fulfilling the second law of thermodynamics, hypoelastic type formulations for the stress and the magnetic field. The main simulation framework is a generic one where both phenomenologically and micromechanically motivated elastic free energy functions that are used for particle-filled magneto-sensitive elastomers can be utilised. The numerical examples presented in our paper demonstrate that the developed approach is suitable to correctly reproduce relevant phenomena observable in curing polymers under a magneto-mechanical coupled loading. Some simplified assumptions like the assumption of a constant temperature and the purely phenomenological character of the presented approach should and will be the subject of a further investigation. An extension for the viscoelasticity and the consideration for the shrinkage effects are going to be dealt in another contribution. After performing these works, there are plans to implement all these model developments in a magneto-mechanical coupled finite element environment in order to perform real life simulations.

Acknowledgements

This work is funded by an ERC advanced grant within the project MOCOPOLY. The authors also express their sincere gratitude to Bastian Walter of the University of Erlangen-Nuremberg for preparation of MRE samples and providing corresponding SEM images used in Fig. 1.

Appendix A

For completeness of our paper, various derivatives appearing in the three stiffness moduli are taken from Otténio et al. (2008). The expressions for the first derivatives of the six invariants with respect to $\boldsymbol{F}$ are,

$$\begin{aligned}
&\frac{\partial I_1}{\partial F_{i\alpha}} = 2F_{i\alpha}, \quad \frac{\partial I_2}{\partial F_{i\alpha}} = 2[C_{\gamma\gamma}F_{i\alpha} - C_{\alpha\gamma}F_{i\gamma}] \\
&\frac{\partial I_3}{\partial F_{i\alpha}} = 2I_3F^{-1}_{i\alpha}, \quad \frac{\partial I_4}{\partial F_{i\alpha}} = 0, \quad \frac{\partial I_5}{\partial F_{i\alpha}} = 2B_\alpha[F_{i\gamma}B_\gamma] \\
&\frac{\partial I_6}{\partial F_{i\alpha}} = 2[F_{i\gamma}B_\gamma C_{\alpha\beta}B_\beta + F_{i\gamma}C_{\gamma\beta}B_\beta B_\alpha]
\end{aligned} \tag{30}$$

and with respect to $\mathbb{B}$ are,

$$\begin{aligned}
&\frac{\partial I_1}{\partial B_\alpha} = 0, \quad \frac{\partial I_2}{\partial B_\alpha} = 0 \quad \frac{\partial I_3}{\partial B_\alpha} = 0 \\
&\frac{\partial I_4}{\partial B_\alpha} = 2B_\alpha, \quad \frac{\partial I_5}{\partial B_\alpha} = 2C_{\alpha\beta}B_\beta, \quad \frac{\partial I_6}{\partial B_\alpha} = 2C_{\alpha\gamma}C_{\gamma\beta}B_\beta.
\end{aligned} \tag{31}$$

The second derivatives of the invariants are computed as follows: first, the second derivatives with respect to $\boldsymbol{F}$,

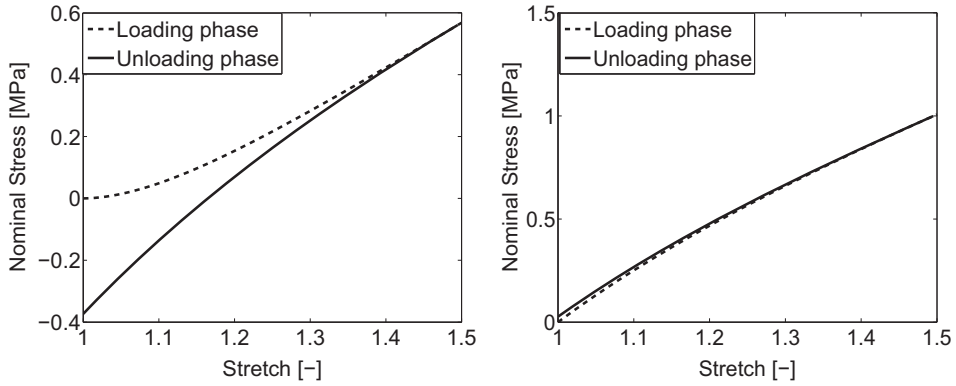

Fig. 14. (Left): stress-stretch relation for time-dependent material parameters as in the curing. (Right) stress-stretch relation produced by constant parameters.

$$
\begin{aligned}
&\frac{\partial^2 I_1}{\partial F_{i\alpha}F_{j\beta}} = 2\delta_{ij}\delta_{\alpha\beta}\\
&\frac{\partial^2 I_2}{\partial F_{i\alpha}F_{j\beta}} = 2[2F_{i\alpha}F_{j\beta} - F_{i\beta}F_{j\alpha} + C_{\gamma\gamma}\delta_{ij}\delta_{\alpha\beta} - b_{ij}\delta_{\alpha\beta} - C_{\alpha\beta}\delta_{ij}]\\
&\frac{\partial^2 I_3}{\partial F_{i\alpha}F_{j\beta}} = 4I_3F^{-1}_{\alpha i}F^{-1}_{\beta j} - 2I_3F^{-1}_{\alpha j}F^{-1}_{\beta i}\\
&\frac{\partial^2 I_4}{\partial F_{i\alpha}F_{j\beta}} = 0\\
&\frac{\partial^2 I_5}{\partial F_{i\alpha}F_{j\beta}} = 2\delta_{ij}B_\alpha B_\beta\\
&\frac{\partial^2 I_6}{\partial F_{i\alpha}F_{j\beta}} = 2[\delta_{ij}[C_{\alpha\gamma}B_\gamma B_\beta + C_{\beta\gamma}B_\gamma B_\alpha] + \delta_{\alpha\beta}F_{i\gamma}B_\gamma F_{j\tau}B_\tau + F_{i\gamma}B_\gamma F_{j\alpha}B_\beta + F_{j\gamma}B_\gamma F_{i\beta}B_\alpha + b_{ij}B_\alpha B_\beta]
\end{aligned}
\tag{32}
$$

next, the mixed derivatives with respect to $\boldsymbol{F}$ and $\mathbb{B}$;

$$
\begin{aligned}
&\frac{\partial^2 I_1}{\partial F_{i\alpha}B_\beta} = 0, \quad \frac{\partial^2 I_2}{\partial F_{i\alpha}B_\beta} = 0, \quad \frac{\partial^2 I_3}{\partial F_{i\alpha}B_\beta} = 0, \quad \frac{\partial^2 I_4}{\partial F_{i\alpha}B_\beta} = 0\\
&\frac{\partial^2 I_5}{\partial F_{i\alpha}B_\beta} = 2\delta_{\alpha\beta}F_{i\gamma}B_\gamma + B_\alpha F_{i\beta}\\
&\frac{\partial^2 I_6}{\partial F_{i\alpha}B_\beta} = 2F_{i\beta}C_{\alpha\gamma}B_\gamma + 2F_{i\gamma}B_\gamma C_{\alpha\beta} + 2F_{i\gamma}C_{\gamma\beta}B_\alpha + 2\delta_{\alpha\beta}F_{i\gamma}C_{\gamma\tau}B_\tau
\end{aligned}
\tag{33}
$$

finally, the second derivatives with respect to $\mathbb{B}$

$$
\begin{aligned}
&\frac{\partial^2 I_1}{\partial B_\alpha B_\beta} = 0, \quad \frac{\partial^2 I_2}{\partial B_\alpha B_\beta} = 0, \quad \frac{\partial^2 I_3}{\partial B_\alpha B_\beta} = 0\\
&\frac{\partial^2 I_4}{\partial B_\alpha B_\beta} = 2\delta_{\alpha\beta}, \quad \frac{\partial^2 I_5}{\partial B_\alpha B_\beta} = 2C_{\alpha\beta}, \quad \frac{\partial^2 I_6}{\partial B_\alpha B_\beta} = 2C_{\alpha\gamma}C_{\gamma\beta}.
\end{aligned}
\tag{34}
$$

In above expressions δ_{ij} is a Kronecker delta and b_{ij} is the left Cauchy-Green (Finger) tensor.

Appendix B

For the uniaxial tension tests presented in Section 5.1, we apply a stretch in the first direction, i.e. $\lambda_1 (= \lambda)$ while the other two directions are free to move. Note that $\lambda_2 = \lambda_3$ is valid only for the reason that $\mathbb{B}$ is applied in the x_1 direction. Otherwise, one has to work through a more general kinematical framework. In order to fill up the entire deformation tensor expressed in Eq. (27), we need to establish a relationship between λ_1 and λ_2 in terms of λ. From Eq. (25), with the help of so-called Voigt notation and applying the condition that the stress P_{22} is zero, we obtain a non-linear relation for the actual value of λ_2,

$$
\begin{aligned}
f(\lambda_2) = {} & [3\kappa + 2\mu - \kappa\lambda^{-2}\lambda^{2,n}]\lambda_2^2 - 2\mu\lambda_2^{2,n} - 2\kappa\lambda_2^2\ln(\lambda) - 4\kappa\lambda_2^2\\
& \times \ln(\lambda_2) + 2\kappa\lambda_2^{2,n}\ln(\lambda) + 4\kappa\lambda_2^{2,n}\ln(\lambda_2) - 2\kappa\lambda_2^{2,n}\\
= {} & 0
\end{aligned}
\tag{35}
$$

where $\lambda^{2,n}$ and $\lambda_2^{2,n}$ are the stretch values at time t_n. In the above equation, λ_2^2 is the second diagonal entry of the tensor $\boldsymbol{C}$. This non-linear equation can be solved using an iterative scheme, e.g. Newton method or its modified versions to get the update value of λ_2. Note that for the sake of simplicity the superscript $n+1$ is omitted.

Appendix C

In order to show whether the proposed hypoelastic formulations may produce any unphysical results such as a stress hysteresis even for elastic loadings, two loading–unloading uniaxial examples are presented. The material parameters for these simulations are taken from Eq. (29) and Table 1. A magneto-mechanical coupled linearly increasing and decreasing loading–unloading cyclic is applied where the maximum values of the mechanical stretch and the magnetic induction are 1.5 and 0.1 T, respectively. At first the relevant material parameters appearing in the models, namely $\mu(t), \kappa(t), m(t)$ and $l(t)$, are taken as time-evolving parameters as in the case of various examples presented in Section 5. For that, during the unloading phase, a large amount of compressive stress is produced when a sample goes back to its original configuration, cf. Fig. (14, left). This is due to the fact that a material becomes stiffer in the unloading phase compared to the loading phase during a curing process. Once we take non-evolving parameters in the simulation, the stress produced in the unloading phase coincides with the loading phase, cf. Fig. (14, right). A slight discrepancy between loading and unloading responses might be due to numerical errors since the values of λ_2 and λ_3 are calculated iteratively as described in Appendix B. Therefore, we comment that the formulations do not lead to any physically wrong results, at least in the case of elastic loadings.

References

Atluri, S.N., 1984. On constitutive relations at finite strains: hypo-elasticity and elasto-plasticity with isotropic and kinematic hardening. Comput. Methods Appl. Mech. Eng. 43, 137–171.

Boczkowska, A., Awietjan, S.F., 2009. Smart composites of urethane elastomers with carbonyl iron. J. Mater. Sci. 44, 4104–4111.

Böse, H., Röder, R., 2009. Magnetorheological elastomers with high variability of their mechanical properties. J. Phy.: Conf. Ser. 149, 012090.

Böse, H., Rabindranath, R., Ehrlich, J., 2012. Soft magnetorheological elastomers as new actuators for valves. J. Intell. Mater. Syst. Struct. 23, 989–994.

Boyce, M.C., Arruda, E.M., 2000. Constitutive models of rubber elasticity: a review. Rubber Chem. Technol. 73, 504–523.

Brigadnov, I.A., Dorfmann, A., 2003. Mathematical modeling of magneto- sensitive elastomers. Int. J. Solids Struct. 40, 4659–4674.

Bustamante, R., 2009. Mathematical modelling of boundary conditions for magneto-sensitive elastomers: variational formulations. J. Eng. Math. 64, 281–301.

Bustamante, R., 2010. Transversely isotropic nonlinear magneto-active elastomers. Acta Mech. 210, 183–214.
Bustamante, R., Dorfmann, A., Ogden, R.W., 2007. A nonlinear magnetoelastic tube under extension and inflation in an axial magnetic field: numerical solution. J. Eng. Math. 59, 139–153.
Chen, L., Gong, X.L., Jiang, W.Q., Yao, J.J., Deng, H.X., Li, W.H., 2007. Investigation on magnetorheological elastomers based on natural rubbers. J. Mater. Sci. 42, 5483–5499.
Danas, K., Kankanala, S.A., Triantafyllidis, 2012. Experiments and modelling of iron-particle-filled magnetorheological elastomers. J. Mech. Phys. Solids 60, 120–138.
Destrade, M., Murphy, J.G., Saccomandi, G., 2012. Simple shear is not so simple. Int. J. Non-Linear Mech. 47 (2), 210–214.
Dorfmann, A., Ogden, R.W., 2003. Magnetoelastic modelling of elastomers. Eur. J. Mech. A Solids 22, 497–507.
Dorfmann, A., Ogden, R.W., 2004. Nonlinear magnetoelastic deformations. Q. J. Mech. Appl. Math. 57, 599–622.
Eringen, A.C., Maugin, G.A., 1990. Electrodynamics of Continua, vol. 1. Springer-Verlag.
Gillen, K.T., 1988. Effect of cross-links which occur during continuous chemical stress-relaxation. Macromolecules 21, 442–446.
Ginder, J.M., Clark, S.M., Schlotter, W.F., Nichols, M.E., 2002. Magnetostrictive phenomena in magnetorheological elastomers. Int. J. Mod. Phys. B. 16, 2412–2418.
Heinrich, C., Aldridge, M., Wineman, A.S., Kieffer, J., Waas, A.M., Shahwan, K.W., 2013. The role of curing stresses in subsequent response, damage and failure of textile polymer composites. J. Mech. Phys. Solids 61, 1241–1264.
Hojjati, M., Johnston, A., Hoa, S.V., Denault, J., 2004. Viscoelastic behaviour of Cytec FM73 adhesive during cure. J. Appl. Polym. Sci. 91, 2548–2557.
Hossain, M., 2010. Modelling and computation of polymer curing (Ph.D. Dissertation), University of Erlangen-Nuremberg, Germany.
Hossain, M., Steinmann, P., 2011. Modelling and simulation of the curing process of polymers by a modified formulation of the Arruda–Boyce model. Arch. Mech. 63 (5–6), 621–633.
Hossain, M., Steinmann, P., 2013. More hyperelastic models for rubber-like materials: consistent tangent operators and comparative study. J. Mech. Behav. Mater. 22 (1–2), 27–50.
Hossain, M., Possart, G., Steinmann, P., 2009a. A small-strain model to simulate the curing of thermosets. Comput. Mech. 43, 769–779.
Hossain, M., Possart, G., Steinmann, P., 2009b. A finite strain framework for the simulation of polymer curing. Part I: elasticity. Comput. Mech. 44 (5), 621–630.
Hossain, M., Possart, G., Steinmann, P., 2010. A finite strain framework for the simulation of polymer curing. Part II: viscoelasticity and shrinkage. Comput. Mech. 46 (3), 363–375.
Jackson, J.D., 1975. Classical Electrodynamics, second ed. John Wiley & Sons, New York.
Jolly, M.R., Carlson, J.D., Muñoz, B.C., 1996. A model of the behaviour of magnetorheological materials. Smart Mater. Struct. 5, 607–614.
Kaleta, J., Krolewicz, M., Lewandowski, D., 2011. Magnetomechanical properties of anisotropic and isotropic magnetorheological composites with thermoplastic elastomer matrices. Smart Mater. Struct. 20, 1–12.
Kankanala, S.A., Triantafyllidis, N., 2004. On finite strain magnetorheological elastomers. J. Mech. Phys. Solids 54, 2869–2908.
Kiasat, M., 2000. Curing shrinkage and residual stresses in viscoelastic thermosetting resins and composites (Ph.D. thesis), TU Delft, The Netherlands.
Klinge, S., Bartels, A., Steinmann, P., 2012a. Modeling of curing processes based on a multi-field potential: single and multi-scale aspects. Int. J. Solids Struct. 49, 2320–2333.
Klinge, S., Bartels, A., Steinmann, P., 2012b. The multi-scale approach to the curing of polymer incorporating viscous and shrinkage effects. Int. J. Solids Struct. 49, 3883–3990.
Liebl, C., Johlitz, M., Yagimli, B., Lion, A., 2012a. Three-dimensional chemo-thermomechanically coupled simulation of curing adhesives including viscoplasticity and chemical shrinkage. Comput. Mech. 49 (5), 603–615.
Liebl, C., Johlitz, M., Yagimli, B., Lion, A., 2012b. Simulation of curing-induced viscoplastic deformation: A new approach considering chemo-thermomechanical coupling. Arch. Appl. Mech. http://dx.doi.org/10.1007/s00419-012-0639-z.
Lion, A., Höfer, P., 2007. On the phenomenological representation of curing phenomena in continuum mechanics. Arch. Mech. 59, 59–89.
Lion, A., Johlitz, M., 2012. On the representation of chemical ageing of rubber in continuum mechanics. Int. J. Solids Struct. 49 (10), 1227–1240.
Lion, A., Yagimli, B., 2008. Differential scanning calorimetry – continuum mechanical considerations with focus to the polymerisation of adhesives. Z. Angew. Math. Mech. 88, 388–402.
Lion, A., Yagimli, B., Baroud, G., Goerke, U., 2008. Constitutive modelling of PMMA-based bone cement: a functional model of viscoelasticity and its approximation for time domain investigations. Arch. Mech. 60, 197–218.
Lokander, M., 2004. Performance of magnetorheological rubber materials (Ph.D. thesis), KTH, Stockholm.
Mahnken, R., 2013. Thermodynamic consistent modeling of polymer curing coupled to viscoelasticity at large strains. Int. J. Solids Struct.
Mergheim, J., Possart, G., Steinmann, P., 2012. Modelling and computation of curing and damage of thermosets. Comput. Mater. Sci. 53, 359–367.
Miehe, C., Kiefer, B., Rosato, D., 2011. An incremental variational formulation of dissipative magnetostriction at the macroscopic continuum level. Int. J. Solids Struct. 48, 1846–1866.
Miehe, C., Rosato, D., Kiefer, D., 2011. Variational principles in dissipative electro-magneto-mechanics: a framework for the macro-modeling of functional materials. Int. J. Numer. Methods Eng. 86, 1225–1276.
Otténio, M., Destrade, M., Ogden, R.W., 2008. Incremental magnetoelastic deformations, with application to surface instability. J. Elast. 90, 19–42.
Pao, Y.H., 1978. Electromagnetic forces in deformable continua. In: Nemat-Nasser, S. (Ed.), Mechanics Today, vol. 4. Oxford University Press, pp. 209–305.
Ruiz, E., Trochu, F., 2005. Thermomechanical properties during cure of glass-polyester RTM composites: elastic and viscoelastic modeling. J. Compos. Mater. 39, 881–916.
Saxena, P., Ogden, R.W., 2011. On surface waves in a finitely deformed magnetoelastic half-space. Int. J. Appl. Mech. 3, 633–665.
Saxena, P., Hossain, M., Steinmann, P., 2013. A theory of finite deformation magneto-viscoelasticity. Int. J. Solids Struct. 50 (24), 3886–3897.
Saxena, P., Hossain, M., Steinmann, P., 2014. Nonlinear magneto-viscoelasticity of transversally isotropic magneto-active polymers. Proc. R. Soc. A 470 (2166).
Spencer, A.J.M., 1971. Theory of invariants. In: Eringen, A.C. (Ed.), Continuum Physics, vol. 1. Academic, New York, pp. 239–353.
Steinmann, P., Hossain, M., Possart, G., 2012. Hyperelastic models for rubber-like materials: consistent tangent operators and suitability for Treloar's data. Arch. Appl. Mech. 82 (9), 1183–1217.
Suzuki, K., Miyano, Y., 1977. Change of viscoelastic properties of epoxy resin in the curing process. J. Appl. Polym. Sci. 21, 3367–3379
Varga, Z., Filipcsei, G., Zrínyi, M., 2006. Magnetic field sensitive functional elastomers with tuneable elastic modulus. Polymer 47, 227–233.
Vogel, F., Bustamante, R., Steinmann, P., 2012. On some mixed variational principles in electro-elastostatics. Int. J. Non-Linear Mech. 47 (2), 341–354.
Vogel, F., Bustamante, R., Steinmann, P., 2013. On some mixed variational principles in magneto-elastostatics. Int. J. Non-Linear Mech. 51, 157–169.
Wriggers, P., 2008. Nonlinear Finite Element Methods. Springer, New York.
Xu, Y., Gonbg, X., Xuan, S., Zhang, W., Fan, Y., 2011. A high-performance magnetorheological material: preparation, characterization and magnetic-mechanic coupling properties. Rheol. Acta 49, 733–740.
Yagimli, B., Lion, A., 2011. Experimental investigations and material modelling of curing processes under small deformations. Z. Angew. Math. Mech. 91, 342–359.
Zhou, G., 2003. Shear properties of a magnetorheological elastomer. Smart Mater. Struct. 12, 139–146.